JGR Planets

RESEARCH ARTICLE
10.1029/2022JE007265

Key Points:

- *D*/*L* scaling analyses revealed new information on the fault growth of the faults affecting Floor-Fractured craters
- The nonlinear relationship between displacement and length, and low D_{max}/L values, can be attributed to linkage and/or vertical restriction
- We introduced a new semiautomated methodology (public and accessible) to help investigate further areas in future works on *D*/*L* analyses

Supporting Information:

Supporting Information may be found in the online version of this article.

Correspondence to:

E. Luzzi,
e.luzzi@jacobs-university.de

Citation:

Luzzi, E., Nodjoumi, G., Massironi, M., Pozzobon, R., & Rossi, A. P. (2023). A semiautomated analysis of displacement-to-length scaling of the grabens affecting lunar floor-fractured craters. *Journal of Geophysical Research: Planets*, *128*, e2022JE007265. https://doi.org/10.1029/2022JE007265

Received 24 FEB 2022
Accepted 4 MAR 2023

Author Contributions:

Conceptualization: Erica Luzzi, Giacomo Nodjoumi, Matteo Massironi, Riccardo Pozzobon, Angelo Pio Rossi
Data curation: Erica Luzzi
Investigation: Erica Luzzi
Methodology: Giacomo Nodjoumi
Software: Giacomo Nodjoumi
Supervision: Matteo Massironi, Riccardo Pozzobon, Angelo Pio Rossi
Writing – original draft: Erica Luzzi
Writing – review & editing: Giacomo Nodjoumi, Matteo Massironi, Riccardo Pozzobon, Angelo Pio Rossi

A Semiautomated Analysis of Displacement-To-Length Scaling of the Grabens Affecting Lunar Floor-Fractured Craters

Erica Luzzi[1,2], Giacomo Nodjoumi[1], Matteo Massironi[3], Riccardo Pozzobon[3,4], and Angelo Pio Rossi[1]

[1]School of Science, Constructor University, Bremen, Germany, [2]Bay Area Environmental Research Institute (BAERI), Moffett Field, CA, USA, [3]Dipartimento di Geoscienze, Università degli Studi di Padova, Padua, Italy, [4]INAF-OAPD, Padua, Italy

Abstract Lunar floor-fractured craters are characterized by the occurrence of radial and concentric grabens, and while their formation mechanism was broadly studied in literature, the relationships between displacement and length of the faults, together with the fault growth, were never examined. We produced a semiautomated Python-based script able to analyze all the parameters required for this study: displacement, length, width of the grabens, and power law relationship between displacement and length. The results of our investigation, carried on in Komarov, Humboldt, and Atlas craters, showed a sublinear fault growth, suggesting that for some reason the increase in displacement is not linear with respect to length. This can result from the interplay of mechanical discontinuities related to the stratigraphy (which cause a vertical fault restriction, preventing the displacement from developing in depth), and to linkage phenomena. The D_{max}/L ratios that resulted from our analyses are higher than previously predicted for the Moon and appear more similar to the values observed on Earth. The slip distribution revealed different stages of fault interaction within the same crater, while the overall maturity of the grabens seems to be significantly high based on the observed symmetry of the grabens. Moreover, our code (public and accessible) can facilitate future works that aim to widen our knowledge about the lunar faults' growth, with all the implications that can improve our understanding of the faults' behavior.

Plain Language Summary Floor-fractured craters are a particular type of lunar craters that present polygonal faults on the floor. Faults are characterized by a certain amount of displacement and a certain length. We can relate these two parameters and study their scaling laws, getting information on the fault growth. Our results, obtained through a new semiautomated methodology that we developed, show a sublinear fault growth in the three studied craters. Sublinear fault growth consists of nonlinear growth between length and displacement, with the latter being prevented from developing in-depth. Such impediment might be caused by a stratigraphic or mechanical barrier beneath the crater that would hamper the displacement of the faults, perhaps indicating a complex geological setting and stratigraphy below and within the crater.

1. Introduction

1.1. Displacement-To-Length Scaling

The correlation between the maximum displacement on a fault (D_{max}) and the fault length (L) has been studied for decades (Cartwright et al., 1995; Clark & Cox, 1996; Cowie & Scholz, 1992a, 1992b; Cox & Scholz, 1988; Dawers & Anders, 1995; Kim & Sanderson, 2005; Muraoka & Kamata, 1983; Peacock & Sanderson, 1991; Poulimenos, 2000; Scholz et al., 1993; R. A. Schultz & Fossen, 2002; Walsh & Watterson, 1988, 1989; Walsh et al., 2002; Wilkins & Gross, 2002; Wojtal, 1996) and later this study has been extended also to terrestrial planets (Byrne et al., 2014; Callihan & Klimczak, 2019; Di Achille et al., 2012; Fernández & Anguita, 2007; Roggon et al., 2017; R. A. Schultz, 1997; R. A. Schultz et al., 2006; Watters et al., 2000; Wyrick et al., 2011).

A power law relationship between displacement and length can be observed in the commonly used Equation 1:

$$D_{max} = \gamma L^{c} \quad (1)$$

where γ is a constant depending on several factors (e.g., lithology, regional stress), and the exponent c depends on the nature of the scaling: a linear scaling law corresponds to $c = 1$, while in the case of scale-dependent geometries c is defined by values $\neq 1$ (Kim & Sanderson, 2005). In cases where the scaling exponent is greater than 1

(e.g., 1.5 or 2), the power law can be defined as superlinear; on the other hand, if the c value is less than 1 (e.g., 0.5), the power law is defined as sublinear (Callihan & Klimczak, 2019; Xu et al., 2016).

The displacement-to-length scaling can shed light on the fault growth mechanism. The two main models for fault growth are described in detail by Cladouhos and Marrett (1996): the first is the individual fault growth, where the lengthening of single faults is due to tips rupture and propagation; the second is the linkage model, where the growth is ascribed to the coalescence of multiple faults within a population. The maximum displacement along the fault generally occurs in the central part of the fault, but in the case of relay (an overlap zone where the displacement is transferred between the overlapping faults) the maximum displacement tends to migrate toward the tips with subsequential connection (Childs et al., 1995). The slip distribution along the fault length provides information on the possible interaction between adjacent faults (Callihan & Klimczak, 2019; Cowie & Scholz, 1992a; Martin & Watters, 2022; Peacock & Sanderson, 1991). In fact, if we correlate the displacement with given lengths of the fault (e.g., −L/2, 0, L/2), the resulting graph can display plateaued or peaked geometries based on the slip distributions. The first can be associated with an intermediate stage of fault growth, characterized by linked segments, or it can be attributed to a restricted fault growth, where a fault is prevented from accumulating displacement as it grows in length; the second can be ascribed either to early or very late stages of fault growth; when instead the peak is found toward the tips of near faults, linkage can be inferred (Callihan & Klimczak, 2019; and references therein). Additionally, strong evidence for linkage phenomena can be observed in correspondence of minima in the displacement distribution, which could be indicative of fault segmentation (Peacock & Sanderson, 1991). The nature of the fault growth and interaction is also reflected in Equation 1, in fact, in single faults the scaling exponent c assumes values close to 1, while in the case of growth by linkage the scaling exponent has typically a value <1.

The D_{max}/L ratio is important for its statistical significance; to date, different lunar D_{max}/L values are still being presented and debated. According to R. A. Schultz et al. (2006), the D_{max}/L ratio for lunar faults should be 4% compared to a fault of the same length on Earth, and the authors found a resulting scaled value of ∼0.001. The authors took into account lunar gravity and mineralogy (and therefore density), and they also define the dependencies of the D_{max}/L ratio on shear stress, Young's modulus, and shear yield strength. Callihan and Klimczak (2019) found that the D_{max}/L ratios on the Moon can result in higher values: they report an average of 0.0121, and a range of individual values spanning from 0.0012 to 0.135. More recently, Martin and Watters (2022) found D_{max}/L ratios spanning from 0.0015 to 0.0176.

Despite the occurrence of the previously mentioned publications, there are aspects of displacement-to-length scaling of the lunar grabens at specific geologic settings that deserve further attention. We apply for the first time such type of study to floor-fractured craters (FFCs), which are peculiar types of craters presenting a flat floor dissected by intersecting dilatant structures generally called grabens, and whose formation remains debated and elusive, as reported in detail in the next section of this work. By understanding the fault growth of these grabens, we can hypothesize the duration of the stress that caused the deformation, as well as contributing to our knowledge of the factors that could have influenced fault growth on the Moon.

For a clear definition of the terms used in this work (displacement, length, and width) we propose a sketch in Figure 1: in the case of lunar grabens, the hanging-wall is the part comprised in between the graben walls. The throw of the fault is the vertical offset created by the movement of the downthrown block; in our case the throw corresponds to the height difference between the surface and the interior of the graben, as shown also in Callihan and Klimczak (2019). The length is measured along the strike of the faults, and the width is the distance between the two faults forming a graben.

1.2. Lunar Floor-Fractured Craters

The FFCs were first recognized by P. H. Schultz (1976) and classified into six different classes based on their distinct morphological characteristics. FFCs display typically radial and/or concentric fractures, and their intersection can produce polygonal blocks. They differ in diameter and features such as central peaks, mare deposits, depth of the floor, bulging, wall terraces, and moats.

More recently, the classification of FFCs was refined by Jozwiak et al. (2012), thanks to the higher resolution of new data.

The FFCs that we selected for this work are Komarov, Humboldt, and Atlas craters (details and location on Table 1).

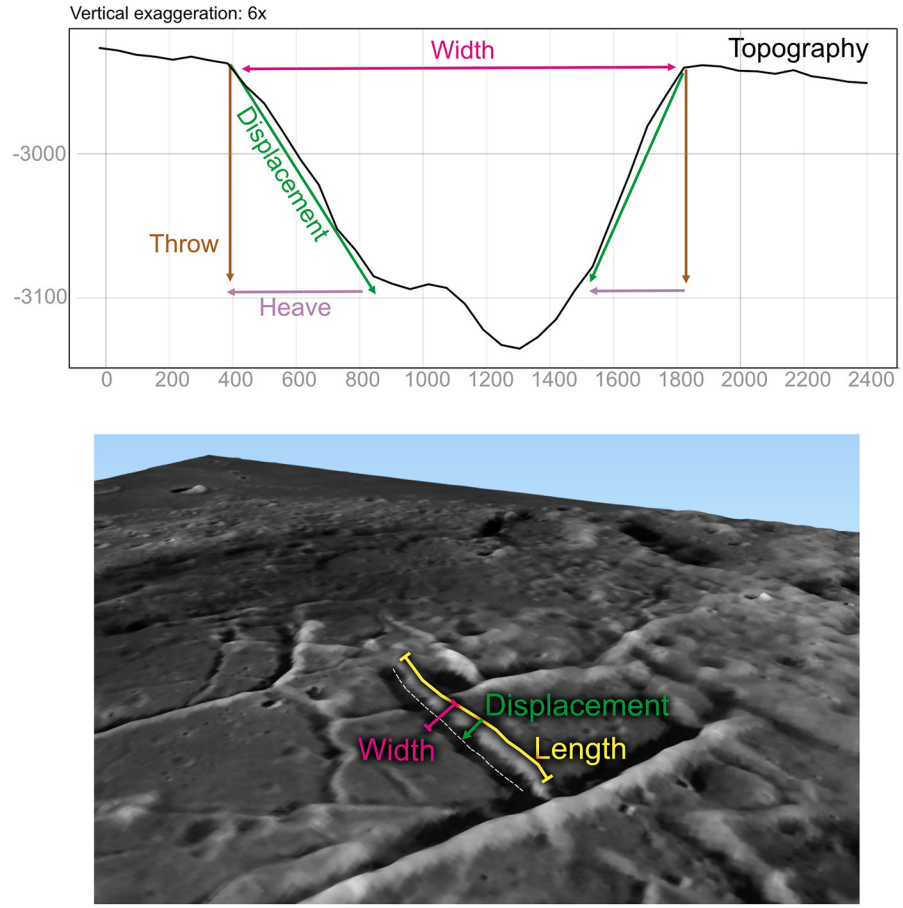

Figure 1. In the top image, the topography along a graben in Humboldt crater is used to show the geometric significance of the used nomenclature; in the bottom image, a 3D scene of Komarov crater is reported to show the length measured along the strike of each fault.

The choice of such craters was mainly due to (a) their large diameter, that can allow us to analyze data at a regional resolution; (b) the fractures in these craters are well visible and are not overprinted by later events; (c) their different stratigraphies, which can give us insights on whether or not lithological contrasts might be a contributing factor for fault growth on the Moon, and to what extent. The FFC classes were not used as selection criteria because some classes do not meet the conditions needed for a numerical approach, and do not present well developed, visible, and/or numerous fractures on the floor that can be measured and assume statistical significance. Instead, we gave priority to Humboldt, Atlas, and Komarov craters, where the occurrence of well visible and dense networks of fractures allowed us to apply the described scaling analyses.

The three studied FFCs have different geological histories:

- In Humboldt crater, as reported by Martinot et al. (2018), the crater central peak complex has a crustal origin, reflected by the widespread occurrence of anorthosite; whereas the walls and the rim show a variety of mafic minerals suggesting the occurrence of preimpact heterogeneities in the crust, either by the emplacement of a pluton or by the deposition of ejecta coming from an adjacent and older crater; the crater floor, where the faults occur, is covered by volcanic deposits that according to the authors could be carefully interpreted as pyroclastic.
- In Komarov crater, the crater floor is flooded by basaltic mare deposits, and the composition is quite homogeneous (Calzada & Mest, 2013; Morota et al., 2009; Thaisen et al., 2011).

Table 1
List of the Studied Floor-Fractured Craters

Crater name	FFC class	Diameter (km)	Latitude (°)	Longitude (°)
Humboldt	1	207	27.14°S	81.15°E
Atlas	1	88	46.44°N	44.22°E
Komarov	3	78	24.27°N	152.22°E

- In Atlas crater, the surface geology is quite complex and characterized by a variety of lithologies, as described by Pathak et al. (2021). According to the authors, the central peak complex is composed of mafic mineralogies, while the crater floor shows both mafic-rich deposits and plagioclase-bearing deposits, as well as two significant pyroclastic patches.

Despite their different stratigraphy, after the deposition of the described deposits, these three craters underwent the same stress that generated the grabens affecting their floors. The formation mechanisms proposed in literature to explain the origin of FFCs are mainly three:

1. Viscous topographic relaxation (Dombard & Gillis, 2001; Hall et al., 1981): it would consist of a rebound of the crater floor following the impact. Because of the viscous properties of the material, after the deformation caused by the impact, the topographic relaxation and subsequent cooling would have generated the characteristic fractures and relief.
2. Emplacement of a magmatic intrusive body underneath the craters (Jozwiak et al., 2012, 2015, 2017; P. H. Schultz, 1976; Thorey et al., 2015; Wilson & Head, 2018): after the emplacement of an intrusive body (generally believed to be a sill/laccolith), the resulting stress would produce the fracturing and the uplift of the crater.
3. Piecemeal caldera collapse (Luzzi et al., 2021): according to the authors, multiple cycles of inflation and deflation of a buried magma chamber can produce the typical polygonal faults observed within chaotic terrains and FFCs.

The evidence presented by Jozwiak et al. (2012) supporting a magmatic intrusion as the formation mechanism of FFCs, and therefore disproving the viscous relaxation, includes: (a) conspicuous floor shallowing, which could not have been produced by viscous relaxation under reasonable lunar conditions; (b) well preserved crater rim crest height, which would have been lowered in case of viscous relaxation; (c) crater asymmetry, attributed to later degradation processes; (d) moats occurring within some FFC classes, which could not have been produced by viscous relaxation in any of the models proposed in literature; (e) FFCs are not located in proximity of basins where thermal anomalies could occur; and (f) many FFCs have diameters <30 km, a diameter range unsupportive of formation by viscous relaxation.

The emplacement of a magmatic body underneath FFCs is currently the most accepted hypothesis for their formation in literature, recently supported also by gravitational data (Jozwiak et al., 2015, 2017; Thorey et al., 2015) and morphometric analyses (Purohit et al., 2021); but it is important to highlight that hypothesis (b) does not necessarily exclude hypothesis (c).

Our work does not intend to provide further confirmation or disapproval of the proposed formation mechanisms, since displacement-to-length scaling alone cannot shed light on the origin of the stress. The goal of this work is to investigate the type of fault growth, hence exploring the possibility of restricted faults and/or linkage processes, and assessing if stratigraphy and lithological contrasts might have played a role during the fault development. Displacement-to-length analyses have never been performed on FFCs, therefore the new data that we present in this work can represent the starting point of an unexplored series of studies, which can be carried on also in future works to better characterize faulting processes within all FFCs.

2. Data and Methods

The imagery used in this work is part of the Lunar Reconnaissance Orbiter Camera Wide Angle Cameras data set (Robinson et al., 2010); the resolution of the images is 75 m/pixel. The Digital Elevation Model (DEM) used for Humboldt and Komarov crater is a merge between the Lunar Orbiter Laser Altimeter (LOLA) and SELenological and Engineering Explorer Kaguya data sets, and the resolution is 59 m/pixel at the equator (Barker et al., 2016), while in Atlas crater, we used the LOLA DEM (Smith et al., 2010) with a resolution of 118 m/pixel, due to an error in this region in the public available data for the merged LOLA-SELENE DEM.

We processed and manipulated the data through a set of six Jupyter Notebooks (Kluyver et al., 2016), two for each crater. One notebook was used to process the data, and the other one to plot the results. All the notebooks are based on Python and open-source python packages, widely used in several applications, including QGIS. We specifically developed these notebooks for this work with the objective of automating functions available in QGIS and its plugins that usually need to be launched manually (Nodjoumi & Luzzi, 2022). The workflow that the code performed for each crater can be summarized as follows (see also Figure 2):

Step 1) The individual faults were manually mapped as linear shapefiles on QGIS. The scale used for mapping ranged between 1:250.000 and 1:150.000 based on the overall size of the mapped fault. When the orthoimage

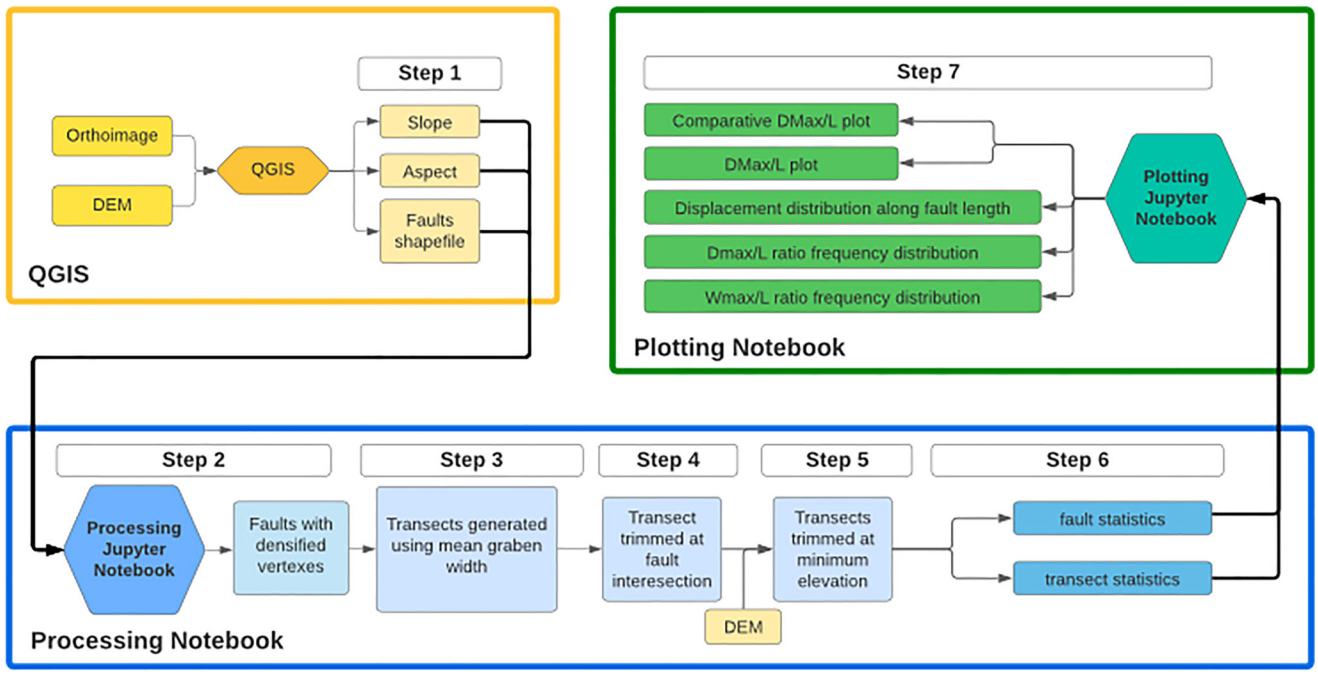

Figure 2. Flowchart depicting the workflow followed by the script. Numbers indicate the order of the processes as listed in the text.

did not have enough resolution for observing specific faults, we instead used the slope map, which represents the rate of change in elevation and can be extrapolated on GIS from a DEM. The slope map helped to distinguish the grabens more clearly as it shows the gradient of a surface, while the imagery alone in some cases can be misleading due to erosion, with sharp margins not perfectly preserved, or to different illumination conditions, which can affect the morphologies' recognition.

Step 2) Since the faults were digitized manually, each geometry is composed of vertexes irregularly spaced between each other. In order to create equally spaced transects along each fault, the processing notebook used the faults shapefile to replace each fault with a new fault composed by equally spaced vertexes. We used the DEMs and the fault lengths to compute the most efficient spacing, resulting in 60 in Komarov, 80 in Atlas, and 120 m in Humboldt.

Step 3) The processing notebook used the densified faults to compute the graben width by calculating the minimum distance between each vertex of a fault and the opposite fault. Then, the notebook generated a transect at each fault vertex using the mean graben width as transect's length.

Step 4) For all faults, the notebook trimmed each transect at the intersection of the transect with the opposite fault.

Step 5) The processing notebook reads the DEM file and combined it with the transect shapefile to generate the topographic profiles and displacement measurements for each transect. To compute the displacement, we used the following 3D distance formula (which is also used by a plugin within QGIS): $\text{cds3d} = \sqrt{(\text{cds2d}_{i+1} - \text{cds2s}_i)^2 + (\text{DEM}_{i+1} - \text{DEM}_i)^2)}$

where:

- cds2d is the progressive 2D distance $= \sqrt{(x_{i+1} - x_i)^2 + (y_{i+1} - y_i)^2}$,
- x, y are the coordinates of the points of the transect
- DEM is the elevation in meters

Step 6) The processing notebook generated faults and transect statistics using the corresponding shapefiles. These statistics include, minimum, maximum, mean, and standard deviation for width and displacement measurements. For the plots, all the data have been scaled in range -1, 1 for x and -1, 1 for y using the scikit-learn MinMaxScaler.

For the classification of the displacement distributions as peaked or plateaued, we applied the quantitative methodology recently proposed by Martin and Watters (2022): the authors used the coefficient of variation (CV),

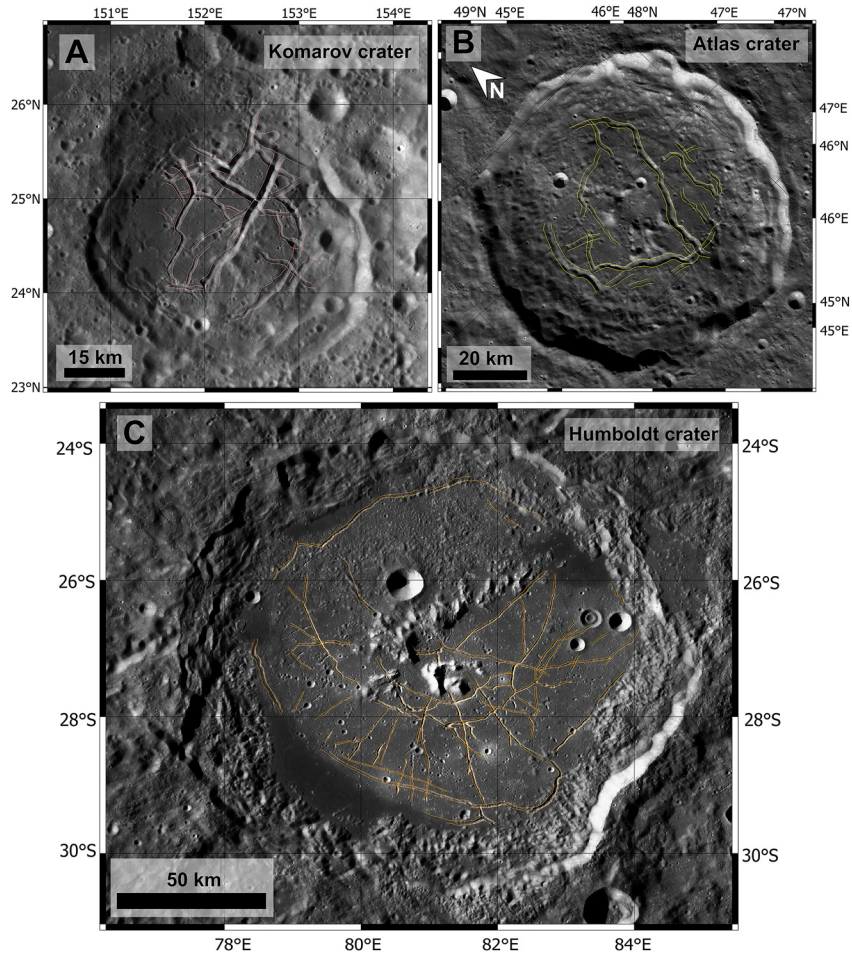

Figure 3. Mapped grabens in (a) Komarov crater, (b) Atlas crater, and (c) Humboldt crater. Lunar Reconnaissance Orbiter Camera Wide Angle Cameras orthoimage. North is up in panels (a and c).

defined as the ratio of the mean to the standard deviation of all the nonzero points in a convex hull fit. The threshold for the classification was set at 2.3 by the authors: values of CV $\geq$ 2.3 correspond to plateaued shapes of displacement, while peaked shapes (referred to as elliptical by the authors) correspond to CV values $<$ 2.3.

3. Results

The final result of the graben's mapping is shown in Figure 3. Some of the structures that at a first glance could resemble grabens, revealed to be pit chains and therefore were not mapped for this study. Where the faults were segmented, we closed the single segments without inferring a buried or hidden continuation, that could jeopardize the accuracy of the fault growth analyses. On the other hand, when the fault was interrupted by a postfaulting impact crater, we inferred the continuation as it was clearly overprinted but present. Following the same reasoning, faults where linkage had been completed were mapped as unique faults, while segments where the linkage was close, but the breaching fault did not form, were mapped as individual segments. Possible linked faults were identified within all the three craters; in most of the cases the linked segments are clearly distinguishable, in other cases the only evidence for linkage is an abrupt drop in the displacement distribution curve. An example from Humboldt crater is presented in Figure 4: along this fault we identified seven major segments, and often the maximum displacement of each segment is located in correspondence of a convex trait of the fault. The major segments can contain minor segments, corresponding to smaller minima in the displacement distribution. The peaks of maximum displacement are observed in the central part of the segment in some cases, while they are shifted toward the tip in other segments. The overall trend of the displacement

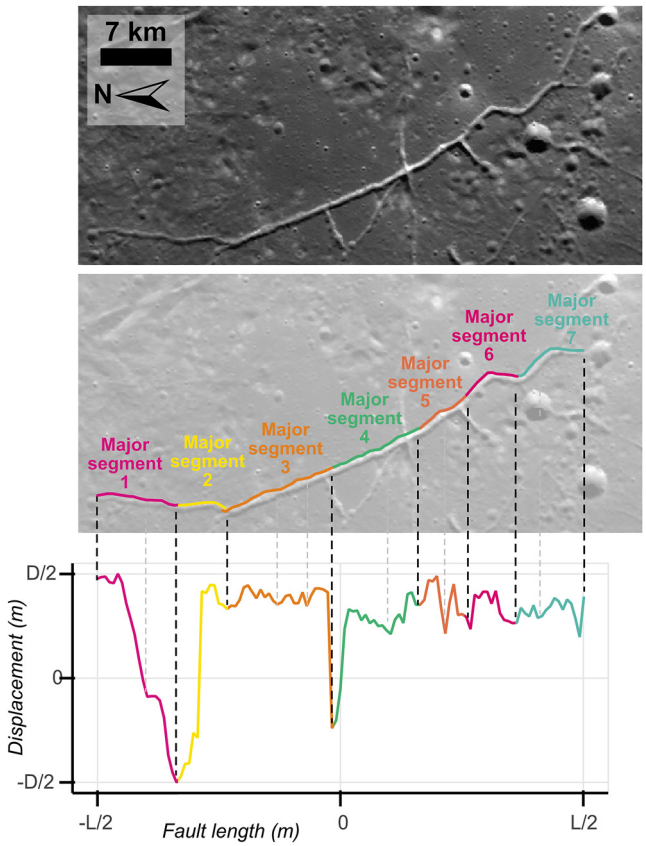

Figure 4. An example of linkage along a fault in Humboldt crater. The drops in the displacement distribution on the bottom of the figure indicate linkage processes, and the corresponding fault segments are highlighted in the line drawing in the middle part of the figure. On the top, the clean orthoimage is shown for context (Lunar Reconnaissance Orbiter Camera-Wide Angle Cameras).

distribution for the total length of the shown fault is constant (except for the minima), suggesting that the relationship between length and displacement is not proportional.

From a morphological point of view, most of the grabens are symmetrical, except a small number of minor grabens, that are barely visible at the available resolution, but that revealed their asymmetry on the slope raster (Figure S1 in Supporting Information S1).

The grabens slightly differ from one crater to another: we observed sharp and large fault traces, especially in Komarov and Humboldt, while in Atlas some of the grabens were too small and therefore less visible.

Interestingly, a major difference was found in the width and displacement of the grabens affecting Humboldt crater, characterized by smaller values compared to Komarov and Atlas.

In fact, the faults in Humboldt crater have a significant length (up to ~66 km, with a mean length of ~24.4 km), while the maximum width along a graben is ~2.7 km (but the average of maximum widths of all the grabens is ~1.2 km, and the average of all widths is 866 m) and the maximum displacement is ~1.8 km. In Komarov crater, faults are long up to ~49 km (mean length ~16.8 km), the maximum width along a fault is ~4.3 km (average maximum width of all the grabens ~2.4 km, and average of all widths ~1.7 km), and the maximum displacement is ~4 km. In Atlas crater, the maximum length of the faults is ~78 km (mean length ~17.5 km), the maximum displacement is ~2.7 km, and the maximum width along a graben is ~2.1 km (average maximum widths of all the grabens ~1.2 km, and average of all widths ~1.1 km). The frequency distributions of maximum width over the length of the faults across the three craters are shown in Figure 5. Detailed measurements of these parameters, including maximum and mean values, are provided in Table S1 (Humboldt), S2 (Komarov), and S3 (Atlas) (supplementary materials).

The concentric pattern of the faults is well visible in all the studied craters, while the radial pattern is more ambiguous in Komarov and Atlas crater and more pronounced in Humboldt crater. Despite these differences, polygonal blocks are formed in all the studied craters, though in Atlas they appear less distinct.

The relationship between maximum displacement and length of the faults is plotted in Figure 6a, while Figure 6b shows how our data distributes in comparison with other data on normal faults from Earth (Corti et al., 2019; Lathrop et al., 2021; Meyer et al., 2002), Mars (Polit et al., 2009), and the Moon (Callihan & Klimczak, 2019; Martin & Watters, 2022) The scaling exponent c results in very low values: 0.31 in Komarov, 0.15 in Humboldt, and 0.27 in Atlas, indicating a sublinear fault growth.

The D_{max}/L ratios (Figure 7) range from 0.012 to 0.449 (mean 0.06) in Humboldt, from 0.045 to 1.086 (mean 0.208) in Komarov, and from 0.032 to 0.376 (mean 0.167) in Atlas (Tables S1, S2, and S3).

The slip distributions along the single faults were plotted to constrain the fault growth through the length and displacement trends, and CV was calculated for each fault to provide a classification as peaked or plateaued. The most exemplifying results are shown in Figure 8, while Figure S2 in Supporting Information S1 shows cases where the classification based on CV appears inconsistent with a visual classification. The classification based on CV for all the distributions in the three studied FFCs is listed in Table S4 in Supporting Information S1.

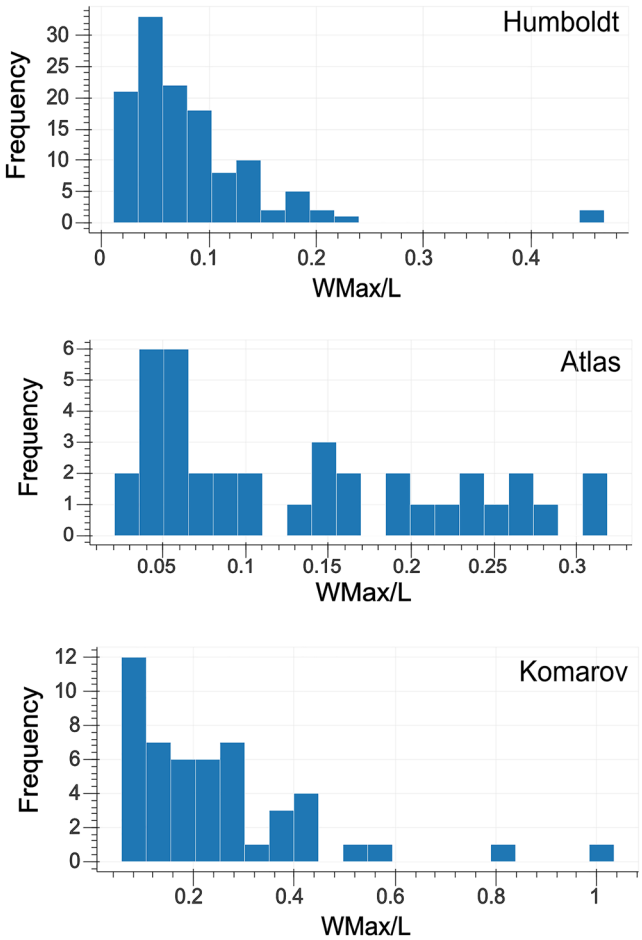

Figure 5. Histograms of the frequency distribution of W_{max}/L values in the studied craters.

4. Discussion

4.1. D_{max}/L Ratios

The results of our scaling analyses revealed higher D_{max}/L ratios than previously proposed for the Moon by R. A. Schultz et al. (2006), and are in accordance with the values proposed more recently by Callihan and Klimczak (2019) and Martin and Watters (2022).

As mentioned, low values of the D_{max}/L ratio (sublinear distribution) indicate a non linear fault growth, where the length grew more than the displacement, suggesting that the fault might be restricted vertically.

As reported in Figure 7, the relationship between maximum displacement and length is far from being proportional, with most of the D_{max}/L values being <0.4 in all three craters, thus suggesting that the displacement along the studied faults did not grow linearly with the length.

The variability of D_{max}/L ratios can depend on multiple factors:

- Mechanical discontinuities (e.g., due to different materials in contact) can act as barriers for the propagation in depth, while laterally the length of the fault can keep growing, therefore causing a vertical fault restriction (Martin & Watters, 2022; Nicol et al., 1996; Wilkins & Gross, 2002);
- Fault segmentation can cause a decrease in D_{max}/L ratios: Atkins et al. (2022) and Xu et al. (2016) found that more segmented faults show a lower D_{max}/L ratio, while individual fault segments accumulated more displacement for a given fault length, and this could be due either to an advanced maturity in the fault's evolution or to the fact that such fault grew in isolation and had no chances of linkage;
- Finally, in case where the fault experiences a reactivation in the opposite sense of slip (and this would be the case if we assume both the inflation first proposed by P. H. Schultz (1976), and the piecemeal caldera collapse suggested by Luzzi et al. (2021)), reverse faults reactivated as normal can show lower values of D_{max}/L ratios (Kim & Sanderson, 2005).

4.2. Displacement Distribution

Despite the fact that in Humboldt and Komarov there seems to be a prevalence of plateaued displacement distributions, peaked distributions are also present, resulting in a variable pattern. In Atlas, most of the distributions were classified as peaked through the methodology based on CV, but plateaued distributions are also present.

In some cases, where the peaks were found toward the tips, we infer an early stage of linkage. In the other cases, linkage processes can be inferred through particular plateaued geometries that, according to Cartwright et al. (1995), show multiple small peaks along a single length and would mainly represent an advanced stage of interaction between more faults. Plateaued distributions are characterized by flat trends that indicate an increase in length and a constant displacement. As previously discussed, and as mentioned by Martin and Watters (2022) and Callihan and Klimczak (2019), this might also be due to mechanical layer thickness confining the fault at depth.

On the other hand, peaked geometries undoubtedly reflect the growth of individual faults, typically having the maximum displacement roughly in the central part of the fault (though sometimes it can be found in more peripheral areas suggesting the beginning of fault interaction). Another implication of this type of slip distribution is also the fact that most likely such faults did not encounter barriers and discontinuities, and were therefore free to grow in depth as well as laterally in length.

In general, the displacement along the mapped faults in the three craters did not show a specific pattern related to their orientation: in some cases, concentric faults had low displacement compared to the length, in other cases, this characteristic is instead occurring along radial faults. In addition, the inner or outer location of the faults

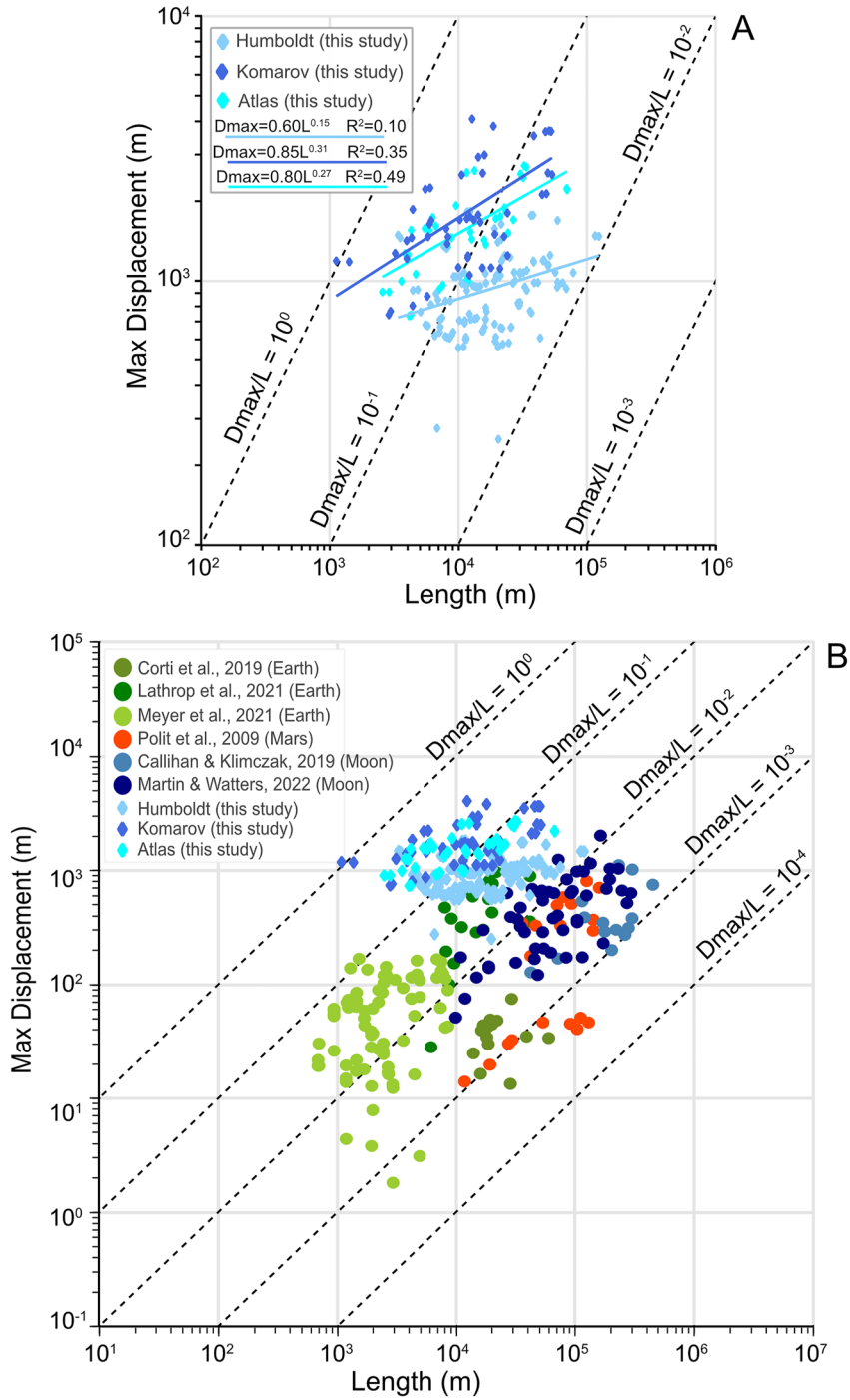

Figure 6. (a) Maximum displacement (D_{max}) and length (L) of the faults are plotted in log-log for each crater, with their respective power law equation. (b) Other extensional faults from previous works (circles) were plotted for a comparison with the data from this study (rhombuses). Green colors indicate terrestrial faults, red indicates Martian faults, and blue colors indicate lunar faults.

with respect to the craters does not seem to have implications on the amount of displacement that the faults accumulated.

An important consideration must be made regarding the applicability of the convex-hull methodology introduced by Martin and Watters (2022) and used in this work to classify the displacement distributions. This type of methodology, together with the triangular/elliptical fit used by Atkins et al. (2022), is one of the first

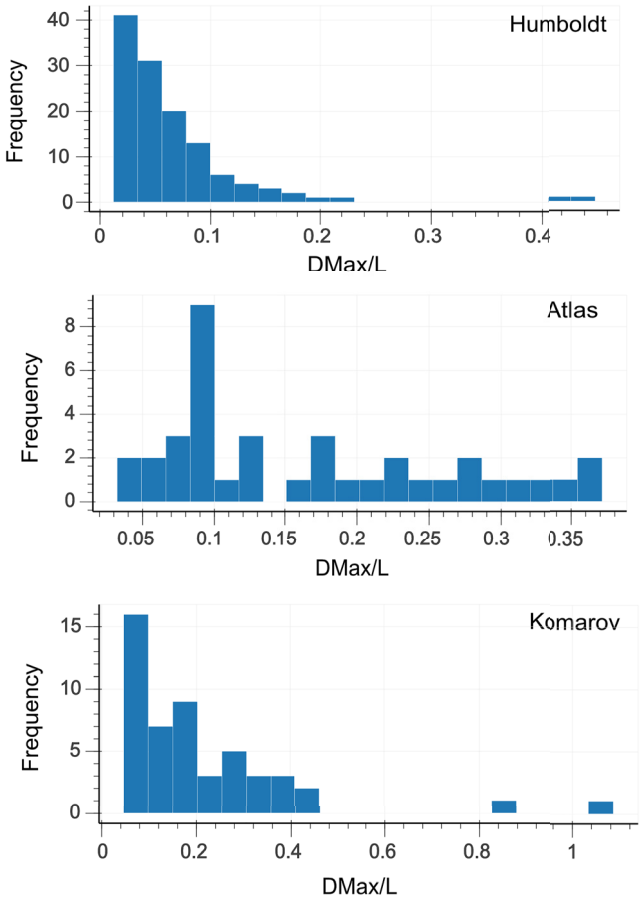

Figure 7. Histograms of the frequency distribution of D_{max}/L values in the studied craters.

attempts to introduce a quantitative classification system for the displacement distributions, and while it constitutes a great contribution in refining displacement-to-length analyses, we found that in our case the results are not always reliable. In fact, while Martin and Watters (2022) found a good fit between the classification based on CV and the visual classification of the plots, our data revealed that the trends classified as peaked in some cases showed a constant displacement along the profile, and vice versa, plateaued profile were actually showing distinct peaks (Figure S2 in Supporting Information S1). These misinterpretations could be due to a variety of factors, including noisy pixels in the DEM, complex interplays of different geological processes, and intersection of faults with different orientations.

4.3. Graben's Width

We observed that in Humboldt, Komarov and Atlas craters, a notable difference regarding the grabens is found in their average width: 866 m in Humboldt, 1.7 in Komarov, and 1.1 km in Atlas. Considering the corresponding lengths and displacements, in Atlas and especially in Humboldt, the width of the grabens seems to be minor compared to Komarov, but the width with respect to the length (Figure 5) is extremely low for all three craters. According to Mège et al. (2003), low width/length ratios of the grabens would be indicative of the formation caused by magmatic intrusion and, assuming the presence of such magmatic intrusion, the width of the grabens would be proportional to the depth of the magmatic body emplaced underneath the grabens (e.g., shallow magmatic bodies would produce narrow grabens). Melosh and Williams (1989) argued that the graben width is mainly controlled by the depth of the initial nucleating fault, rather than by the depth of stratigraphic/mechanical discontinuities, as proposed by Golombek (1979). If we assume that the width of the grabens depends on the depth of the initial faults as proposed by Melosh and Williams (1989), a consideration must be made regarding the depth of the hypothesized magmatic body underneath, and its correlation with crustal thickness in the region. In fact, whether such a magmatic body is a sill/laccolith, as hypothesized by a variety of authors (Jozwiak et al., 2012, 2015, 2017; P. H. Schultz, 1976; Thorey et al., 2015; Wilson & Head, 2018), or it is a magma chamber as recently proposed by Luzzi et al. (2021), its depth might influence the depth of the initial faults, and the width of the grabens (Mège et al., 2003). In Komarov crater, where we observed a slightly larger width of the grabens, the crustal thickness has been predicted to span from 1 to 20 km by Wieczorek et al. (2013), based on Gravity Recovery and Interior Laboratory data. We might speculate that a thin crust beneath FFCs could influence the depth of the initial faults, and therefore the width of the grabens. Nevertheless, Wieczorek et al. (2013) predicted a crustal thickness <5 km in the region of the Humboldt crater, where the grabens' width appears to be lower than in Komarov. In Atlas, where the width of the grabens has values in between Komarov's and Humboldt's, the predicted crustal thickness is 27 km (Wieczorek et al., 2013). In the cases of Komarov and Humboldt craters, the low crustal thickness suggests that the impact might have excavated into the mantle, enhancing intrusive magmatic processes and consequent emplacement of magmatic bodies (Hikida & Wieczorek, 2007; Neumann et al., 1996; Wieczorek et al., 2013). If we assume that initial faulting would have nucleated at a maximum depth corresponding to the crust-mantle interface as suggested by Andrews-Hanna et al. (2018) for the Orientale basin, then the difference between Komarov and Humboldt should not be so significant, and the most extreme difference should have been observed in Atlas crater. Therefore, we can exclude that the depth of initial faulting is solely responsible for the different graben widths. On the other hand, we cannot exclude the interplay of the initial faulting depth and the occurrence of mechanical discontinuities buried in the stratigraphy or, as suggested by Golombek (1979), the latter alone. According to the author, the initial width of the graben increases due to brittle or ductile extension of the rocks underlying the mechanical discontinuity. Since the three studied craters have different geology and stratigraphy, and since such discontinuity is most likely at different depths, this could explain why the widths are different in each crater.

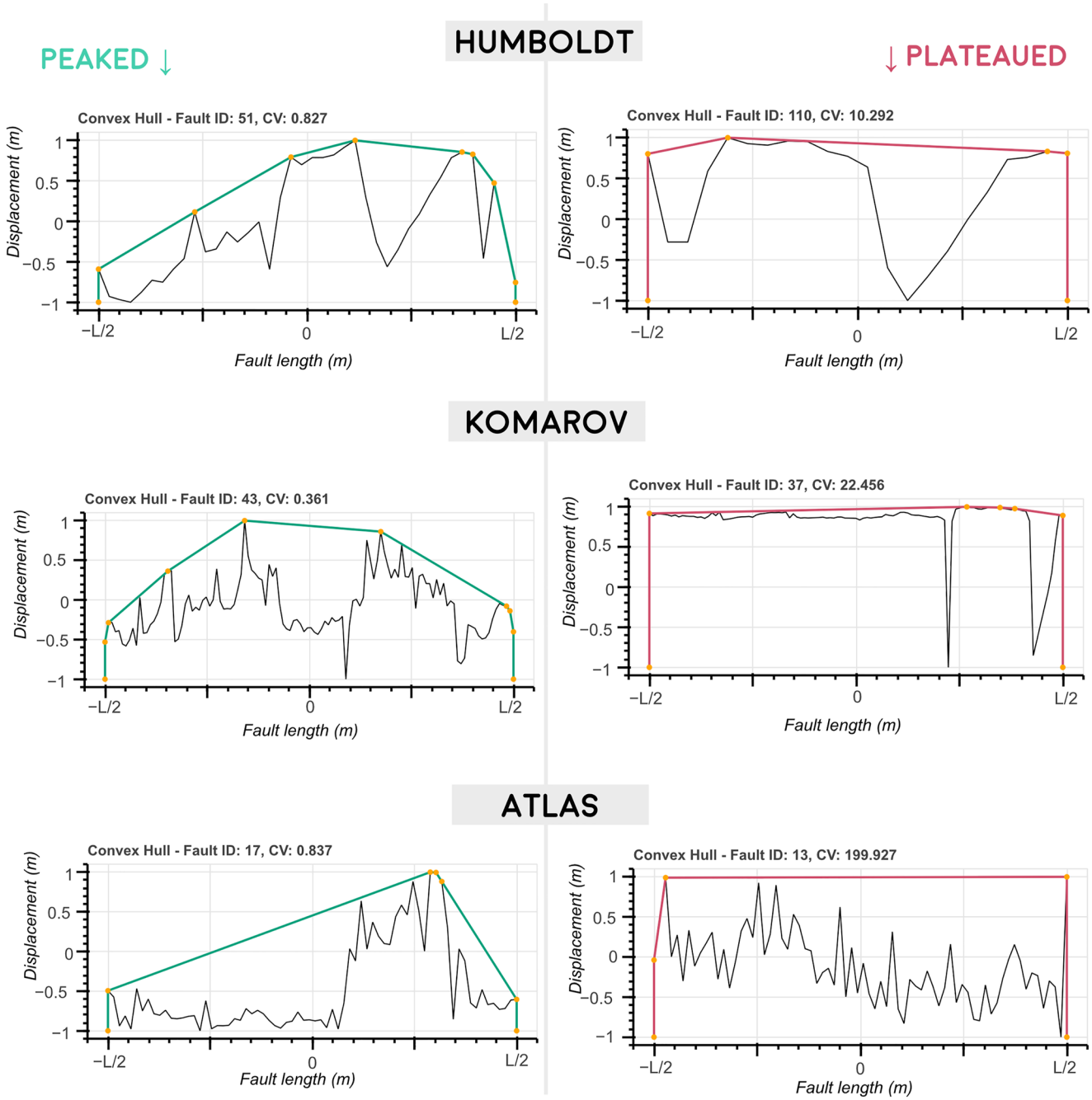

Figure 8. Some examples of the different displacement distributions in the three craters are shown. The colored lines represent the convex hull fit. On the left, peaked distributions are displayed and on the right, plateaued distributions (for each crater). The coefficient of variation value is reported on top of each plot.

4.4. Role of Lithology/Stratigraphy and Its Significance for D_{max}/L Studies

As we mentioned before, Wilkins and Gross (2002) explored the possibility that different types of lithology composing a complex stratigraphy might influence the growth of faults. The authors studied an area in Utah, where the stratigraphy was mainly composed of alternations of shales and sands, and they found that fault tips and minimum value of displacement occur at the lithological contacts. Despite the impossibility to have well or seismic data on the Moon and observe the lithologies occurring in depth, several authors constrained the geological units on the surface in the three studied craters:

1. In Humboldt crater, the findings reported by Martinot et al. (2018) regarding the stratigraphy within this FCC are critical to assess the possibility that in depth pyroclastic and crustal deposits might be in contact through discontinuities that did not allow the faults to grow in depth; this would explain the sublinear growth that we found with the D_{max}/L scaling. In fact, while the fault could grow laterally given the sufficient extent of the pyroclastic deposits, the displacement might have been inhibited by a contact in depth between the central peak complex (and underlying crustal material) and the pyroclastic deposits.
2. In Komarov crater, where basaltic mare deposits result in a homogeneous composition of the crater floor (Calzada & Mest, 2013; Morota et al., 2009; Thaisen et al., 2011), we can hypothesize that such homogeneity might be responsible for the observed higher scaling exponent, meaning that the displacement in Komarov increases more with respect to the length compared to the other two craters.
3. In Atlas crater, as in Humboldt, the complex stratigraphy (Pathak et al., 2021) might explain the very low scaling exponent, associated with a mild increase in displacement with respect to significant lengths of the faults, if we assume that the contacts between different lithologies can act as barriers for the development of the faults in depth.

Radar analyses investigating the subsurface stratigraphy would help determine if and how the inferred mechanical discontinuities influenced the fault growth in the studied areas; unfortunately, to date such study has not been carried out in Atlas, Humboldt, and Komarov craters, but future works and new data sets might shed light on the thickness of the different units, and clarify the relationship between restricted faults and mechanical discontinuities buried below FFCs.

4.5. Linkage and Fault Interaction

Linked segments were identified in all three craters (Figure 4), and the displacement distribution minima confirm that the faults of the studied FFCs interacted and linked. Different degrees of interaction were observed: in some cases the breaching fault did not occur, but the overlap was visible and the area presented minor fractures; in other cases the linkage has been completed resulting in a long fault, where the total displacement did not increment significantly.

Linkage processes have been widely studied in literature (e.g., Atkins et al., 2022; Dawers & Anders, 1995; Kim & Sanderson, 2005; Manighetti et al., 2015; Peacock & Sanderson, 1991; Wilkins & Gross, 2002), and the effect of linkage on D_{max}/L values appears evident both in terrestrial and planetary faults: low D_{max}/L values suggest that a large displacement was not accumulated on segmented faults, while isolated faults tend to exhibit larger displacements and therefore a higher D_{max}/L value. Although Dawers and Anders (1995) propose that faults keep accumulating displacement after the connection of different segments, our results and particularly the widespread low D_{max}/L values suggest that at some point the displacement ceased to develop in depth. Nevertheless, this could be due to vertical fault restriction caused by a heterogeneous stratigraphy, as mentioned before.

4.6. Symmetry of Grabens

By analyzing the symmetry of the grabens, we can infer whether the system might be mature (symmetric) or less mature (asymmetric). Callihan and Klimczak (2019) analyzed several grabens on the Moon and were able to distinguish different areas where the timing and rate of tectonics might have differed. In our case, almost every fault is identical to the correspondent opposite fault, resulting in an overall symmetry. Thus, if we assume that a mature system corresponds to a stress that lasted over a significant amount of time, multiple cycles of inflation and deflation (as suggested by Luzzi et al. (2021)) might be more likely to explain such maturity rather than a single episode of inflation. Luzzi et al. (2021) performed a series of experiments reproducing multiple cycles of inflation and deflation of a buried magma chamber underlying brittle materials. The authors observed that after the second cycle, only minor faults were forming. These small grabens that were formed during the last inflation-deflation, might be analogous of the few small asymmetric grabens that we observed in this study. Nevertheless, this hypothesis needs further attention in future works to be confirmed.

5. Conclusive Remarks

The new python-based methodology introduced in this work allowed us to perform (with minimal user input) the displacement-to-length scaling of the grabens affecting the three lunar FFCs (Komarov, Humboldt, and Atlas), and the results showed a sublinear fault growth, suggesting that the displacement of the studied faults did not

increase linearly with the length. The sublinear fault growth was inferred from the scaling exponent c, that in each crater had a value less than 1. In fact, our analyses revealed the following power law equations: $D_{max} = 0.85L^{0.31}$ in Komarov crater, $D_{max} = 0.60L^{0.15}$ in Humboldt crater, and $D_{max} = 0.80L^{0.27}$ in Atlas crater. The highest scaling exponent and D_{max}/L ratio was found in Komarov crater, where the surface geology is characterized by a homogeneous basaltic lithology, therefore we hypothesize that heterogeneous stratigraphic settings might influence the development of the faults in depth by causing a vertical restriction. Additionally, our results suggest that linkage phenomena and interaction between faults influenced the D_{max}/L values: our interpretation is that after the connection of different segments, the faults did not keep accumulating significant amounts of displacement (probably due to vertical restriction), while the length has been increased by the linkage itself. The slip distributions revealed both plateaued and peaked distributions, indicating different stages of fault interaction within the same crater and/or fault restriction. Finally, the widespread symmetry of the grabens suggests a significant maturity of the grabens system, and this could be explained by a long-lasting stress, either constant or with multiple phases.

This kind of analysis can provide a good amount of information, and through our script, more areas can be investigated in the future to provide a more comprehensive overview of the faults' behavior on the Moon and on terrestrial planets.

Data Availability Statement

All the data used in this work, including imagery, DEMs, slope map, and shapefiles, can be found in a repository following the FAIR principles (Luzzi et al., 2022), while the code for the Jupyter notebooks used for our analyses can be found in Nodjoumi and Luzzi (2022).

Acknowledgments
This work was supported and funded by the European Union's Horizon 2020 research and innovation programme under Grant 776276 (PLANMAP). Open Access funding enabled and organized by Projekt DEAL.

References

Andrews-Hanna, J. C., Head, J. W., Johnson, B. C., Keane, J. T., Kiefer, W. S., McGovern, P. J., et al. (2018). Ring faults and ring dikes around the Orientale basin on the Moon. *Icarus*, *310*, 1–20. https://doi.org/10.1016/j.icarus.2017.12.012

Atkins, R. M., Byrne, P. K., Bohnenstiehl, D. R., & Wegmann, K. W. (2022). A morphometric investigation of large-scale crustal shortening on Mars. *Journal of Geophysical Research: Planets*, *127*(5), e2021JE007110. https://doi.org/10.1029/2021JE007110

Barker, M. K., Mazarico, E., Neumann, G. A., Zuber, M. T., Haruyama, J., & Smith, D. E. (2016). A new lunar digital elevation model from the Lunar Orbiter Laser Altimeter and SELENE Terrain Camera. *Icarus*, *273*, 346–355. https://doi.org/10.1016/j.icarus.2015.07.039

Byrne, P. K., Klimczak, C., Celâl Şengör, A. M., Solomon, S. C., Watters, T. R., & Hauck, S. A. (2014). Mercury's global contraction much greater than earlier estimates. https://doi.org/10.1038/NGEO2097

Callihan, M. B., & Klimczak, C. (2019). Topographic expressions of lunar graben. *Geological Society of America Litosphere*, *11*(2), 294–305. https://doi.org/10.1130/L1025.1

Calzada, A., & Mest, S. C. (2013). Scientific characterization of mare moscoviense region of interest. In *European Planetary Sciences Conference*. (Vol. 8, p. 167).

Cartwright, J. A., Trudgill, B. D., & Mansfield, C. S. (1995). Fault growth by segment linkage: An explanation for scatter in maximum displacement and trace length data from the Canyonlands Grabens of SE Utah. *Journal of Structural Geology*, *17*(9), 1319–1326. https://doi.org/10.1016/0191-8141(95)00033-A

Childs, C., Watterson, J., & Walsh, J. J. (1995). Fault overlap zones within developing normal fault systems. *Journal of the Geological Society*, *152*(3), 535–549. https://doi.org/10.1144/gsjgs.152.3.0535

Cladouhos, T. T., & Marrett, R. (1996). Are fault growth and linkage models consistent with power-law distributions of fault lengths? *Journal of Structural Geology*, *18*(2–3), 281–293. https://doi.org/10.1016/S0191-8141(96)80050-2

Clark, R. M., & Cox, S. J. D. (1996). A modern regression approach to determining fault displacement-length scaling relationships. *Journal of Structural Geology*, *18*(2–3), 147–152. https://doi.org/10.1016/S0191-8141(96)80040-X

Corti, G., Cioni, R., Franceschini, Z., Sani, F., Scaillet, S., Molin, P., et al. (2019). Aborted propagation of the Ethiopian rift caused by linkage with the Kenyan rift. *Nature Communications*, *10*(1), 1–11. https://doi.org/10.1038/s41467-019-09335-2

Cowie, P. A., & Scholz, C. H. (1992a). Displacement-length scaling relationship for faults: Data synthesis and discussion. *Journal of Structural Geology*, *14*(10), 1149–1156. https://doi.org/10.1016/0191-8141(92)90066-6

Cowie, P. A., & Scholz, C. H. (1992b). Physical explanation for the displacement-length relationship of faults using a post-yield fracture mechanics model. *Journal of Structural Geology*, *14*(10), 1133–1148. https://doi.org/10.1016/0191-8141(92)90065-5

Cox, S. J. D., & Scholz, C. H. (1988). On the formation and growth of faults: An experimental study. *Journal of Structural Geology*, *10*(4), 413–430. https://doi.org/10.1016/0191-8141(88)90019-3

Dawers, N. H., & Anders, M. H. (1995). Displacement-length scaling and fault linkage. *Journal of Structural Geology*, *17*(5), 607–614. https://doi.org/10.1016/0191-8141(94)00091-D

Di Achille, G., Popa, C., Massironi, M., Mazzotta Epifani, E., Zusi, M., Cremonese, G., & Palumbo, P. (2012). Mercury's radius change estimates revisited using MESSENGER data. *Icarus*, *221*(1), 456–460. https://doi.org/10.1016/J.ICARUS.2012.07.005

Dombard, A. J., & Gillis, J. J. (2001). Testing the viability of topographic relaxation as a mechanism for the formation of lunar floor-fractured craters. *Journal of Geophysical Research*, *106*(E11), 27901–27909. https://doi.org/10.1029/2000JE001388

Fernández, C., & Anguita, F. (2007). Oblique rifting at tempe fossae, Mars. *Journal of Geophysical Research*, *112*(9), 9007. https://doi.org/10.1029/2007JE002889

Golombek, M. P. (1979). Structural analysis of lunar grabens and the shallow crustal structure of the Moon. *Journal of Geophysical Research*, *84*(B9), 4657. https://doi.org/10.1029/jb084ib09p04657

Hall, J. L., Solomon, S. C., & Head, J. W. (1981). Lunar floor-fractured craters: Evidence for viscous relaxation of crater topography. *Journal of Geophysical Research*, *86*(B10), 9537–9552. https://doi.org/10.1029/jb086ib10p09537

Hikida, H., & Wieczorek, M. A. (2007). Crustal thickness of the Moon: New constraints from gravity inversions using polyhedral shape models. *Icarus*, *192*(1), 150–166. https://doi.org/10.1016/j.icarus.2007.06.015

Jozwiak, L. M., Head, J. W., Neumann, G. A., & Wilson, L. (2017). Observational constraints on the identification of shallow lunar magmatism: Insights from floor-fractured craters. *Icarus*, *283*, 224–231. https://doi.org/10.1016/j.icarus.2016.04.020

Jozwiak, L. M., Head, J. W., & Wilson, L. (2015). Lunar floor-fractured craters as magmatic intrusions: Geometry, modes of emplacement, associated tectonic and volcanic features, and implications for gravity anomalies. *Icarus*, *248*, 424–447. https://doi.org/10.1016/j.icarus.2014.10.052

Jozwiak, L. M., Head, J. W., Zuber, M. T., Smith, D. E., & Neumann, G. A. (2012). Lunar floor-fractured craters: Classification, distribution, origin and implications for magmatism and shallow crustal structure. *Journal of Geophysical Research*, *117*(11), E11005. https://doi.org/10.1029/2012JE004134

Kim, Y. S., & Sanderson, D. J. (2005). The relationship between displacement and length of faults: A review. *Earth-Science Reviews*, *68*(3–4), 317–334. https://doi.org/10.1016/j.earscirev.2004.06.003

Kluyver, T., Ragan-Kelley, B., Pérez, F., Granger, B., Bussonnier, M., Frederic, J., et al. (2016). Jupyter notebooks – A publishing format for reproducible computational workflows. In *Positioning and power in academic publishing: Players, agents and agendas - Proceedings of the 20th international conference on electronic publishing, ELPUB*, (Vol. 2016, pp. 87–90). https://doi.org/10.3233/978-1-61499-649-1-87

Lathrop, B. A., Jackson, C. A. L., Bell, R. E., & Rotevatn, A. (2021). Normal fault kinematics and the role of lateral tip retreat: An example from offshore NW Australia. *Tectonics*, *40*(5), e2020TC006631. https://doi.org/10.1029/2020TC006631

Luzzi, E., Nodjoumi, G., Massironi, M., Pozzobon, R., & Rossi, A. P. (2022). Dataset: A semiautomated analysis of displacement-to-length scaling of the grabens affecting lunar floor-fractured craters. *Zenodo*. https://doi.org/10.5281/zenodo.7503302

Luzzi, E., Rossi, A. P., Massironi, M., Pozzobon, R., Corti, G., & Maestrelli, D. (2021). Caldera collapse as the trigger of chaos and fractured craters on the moon and Mars. *Geophysical Research Letters*, *48*(11), e2021GL092436. https://doi.org/10.1029/2021GL092436

Manighetti, I., Caulet, C., De Barros, L., Perrin, C., Cappa, F., & Gaudemer, Y. (2015). Generic along-strike segmentation of Afar normal faults, East Africa: Implications on fault growth and stress heterogeneity on seismogenic fault planes. *Geochemistry, Geophysics, Geosystems*, *16*(2), 443–467. https://doi.org/10.1002/2014GC005691

Martin, E. S., & Watters, T. R. (2022). Displacement-length scaling relations of nearside graben: Evidence of restricted normal faults on the Moon. *Icarus*, *388*, 115215. https://doi.org/10.1016/J.ICARUS.2022.115215

Martinot, M., Besse, S., Flahaut, J., Quantin-Nataf, C., Lozac'h, L., & van Westrenen, W. (2018). Mineralogical diversity and geology of Humboldt crater derived using moon mineralogy mapper data. *Journal of Geophysical Research: Planets*, *123*(2), 612–629. https://doi.org/10.1002/2017JE005435

Mège, D., Cook, A. C., Garel, E., Lagabrielle, Y., & Cormier, M. H. (2003). Volcanic rifting at Martian grabens. *Journal of Geophysical Research*, *108*(5), 10–11. https://doi.org/10.1029/2002je001852

Melosh, H. J., & Williams, C. A. (1989). Mechanics of graben formation in crustal rocks: A finite element analysis. *Journal of Geophysical Research*, *94*(B10), 13961–13973. https://doi.org/10.1029/jb094ib10p13961

Meyer, V., Nicol, A., Childs, C., Walsh, J. J., & Watterson, J. (2002). Progressive localisation of strain during the evolution of a normal fault population. *Journal of Structural Geology*, *24*(8), 1215–1231. https://doi.org/10.1016/S0191-8141(01)00104-3

Morota, T., Haruyama, J., Honda, C., Ohtake, M., Yokota, Y., Kimura, J., et al. (2009). Mare volcanism in the lunar farside Moscoviense region: Implication for lateral variation in magma production of the Moon. *Geophysical Research Letters*, *36*(21), L21202. https://doi.org/10.1029/2009GL040472

Muraoka, H., & Kamata, H. (1983). Displacement distribution along minor fault traces. *Journal of Structural Geology*, *5*(5), 483–495. https://doi.org/10.1016/0191-8141(83)90054-8

Neumann, G. A., Zuber, M. T., Smith, D. E., & Lemoine, F. G. (1996). The lunar crust: Global structure and signature of major basins. *Journal of Geophysical Research*, *101*(E7), 16841–16863. https://doi.org/10.1029/96JE01246

Nicol, A., Watterson, J., Walsh, J. J., & Childs, C. (1996). The shapes, major axis orientations and displacement patterns of fault surfaces. *Journal of Structural Geology*, *18*(2–3), 235–248. https://doi.org/10.1016/S0191-8141(96)80047-2

Nodjoumi, G., & Luzzi, E. (2022). FAS: Faults automated scaling. https://doi.org/10.5281/ZENODO.7472818

Pathak, S., Dagar, A. K., Bhattacharya, S., Moitra, H., Chauhan, M., & Gupta, S. (2021). Geological insights into lunar floor-fractured crater Atlas. *Icarus*, *360*, 114374. https://doi.org/10.1016/j.icarus.2021.114374

Peacock, D. C. P., & Sanderson, D. J. (1991). Displacements and segment linkage in strike-slip fault zones. *Journal of Structural Geology*, *13*(9), 1025–1035. https://doi.org/10.1016/0191-8141(91)90054-M

Polit, A. T., Schultz, R. A., & Soliva, R. (2009). Geometry, displacement-length scaling, and extensional strain of normal faults on Mars with inferences on mechanical stratigraphy of the Martian crust. *Journal of Structural Geology*, *31*(7), 662–673. https://doi.org/10.1016/j.jsg.2009.03.016

Poulimenos, G. (2000). Scaling properties of normal fault populations in the western Corinth Graben, Greece: Implications for fault growth in large strain settings. *Journal of Structural Geology*, *22*(3), 307–322. https://doi.org/10.1016/S0191-8141(99)00152-2

Purohit, S., Gandhi, S., Dubey, N., & Chauhan, P. (2021). Quantitative validation of formation mechanism of lunar floor fractured craters. In *International geoscience and remote sensing symposium (IGARSS)*, (pp. 6618–6621). https://doi.org/10.1109/IGARSS47720.2021.9554472

Robinson, M. S., Brylow, S. M., Tschimmel, M., Humm, D., Lawrence, S. J., Thomas, P. C., et al. (2010). Lunar reconnaissance orbiter camera (LROC) instrument overview. *Space Science Reviews*, *150*(1–4), 81–124. https://doi.org/10.1007/s11214-010-9634-2

Roggon, L., Hetzel, R., Hiesinger, H., Clark, J. D., Hampel, A., & van der Bogert, C. H. (2017). Length-displacement scaling of thrust faults on the Moon and the formation of uphill-facing scarps. *Icarus*, *292*, 111–124. https://doi.org/10.1016/j.icarus.2016.12.034

Scholz, C. H., Dawers, N. H., Yu, J. Z., Anders, M. H., & Cowie, P. A. (1993). Fault growth and fault scaling laws: Preliminary results. *Journal of Geophysical Research*, *98*(B12), 21951–21961. https://doi.org/10.1029/93jb01008

Schultz, P. H. (1976). Floor-fractured lunar craters. *The Moon*, *15*(3–4), 241–273. https://doi.org/10.1007/BF00562240

Schultz, R. A. (1997). Displacement-length scaling for terrestrial and Martian faults: Implications for Valles Marineris and shallow planetary grabens. *Journal of Geophysical Research*, *102*(6), 12009–12015. https://doi.org/10.1029/97jb00751

Schultz, R. A., & Fossen, H. (2002). Displacement-length scaling in three dimensions: The importance of aspect ratio and application to deformation bands. *Journal of Structural Geology*, *24*(9), 1389–1411. https://doi.org/10.1016/S0191-8141(01)00146-8

Schultz, R. A., Okubo, C. H., & Wilkins, S. J. (2006). Displacement-length scaling relations for faults on the terrestrial planets. *Journal of Structural Geology*, *28*(12), 2182–2193. https://doi.org/10.1016/j.jsg.2006.03.034

Smith, D. E., Zuber, M. T., Neumann, G. A., Lemoine, F. G., Mazarico, E., Torrence, M. H., et al. (2010). Initial observations from the lunar orbiter laser altimeter (LOLA). *Geophysical Research Letters*, *37*(18), 18204. https://doi.org/10.1029/2010GL043751

Thaisen, K. G., Head, J. W., Taylor, L. A., Kramer, G. Y., Isaacson, P., Nettles, J., et al. (2011). Geology of the moscoviense basin. *Journal of Geophysical Research*, *116*(E6), E00G07. https://doi.org/10.1029/2010JE003732

Thorey, C., Michaut, C., & Wieczorek, M. (2015). Gravitational signatures of lunar floor-fractured craters. *Earth and Planetary Science Letters*, *424*, 269–279. https://doi.org/10.1016/j.epsl.2015.04.021

Walsh, J. J., Nicol, A., & Childs, C. (2002). An alternative model for the growth of faults. *Journal of Structural Geology*, *24*(11), 1669–1675. https://doi.org/10.1016/S0191-8141(01)00165-1

Walsh, J. J., & Watterson, J. (1988). Analysis of the relationship between displacements and dimensions of faults. *Journal of Structural Geology*, *10*(3), 239–247. https://doi.org/10.1016/0191-8141(88)90057-0

Walsh, J. J., & Watterson, J. (1989). Displacement gradients on fault surfaces. *Journal of Structural Geology*, *11*(3), 307–316. https://doi.org/10.1016/0191-8141(89)90070-9

Watters, T. R., Schultz, R. A., & Robinson, M. S. (2000). Displacement length relations of trust faults associated with lobate scarps on Mercury and Mars comparison with terrestrial faults. *Geophysical Research Letters*, *27*(22), 3659–3662. https://doi.org/10.1029/2000GL011554

Wieczorek, M. A., Neumann, G. A., Nimmo, F., Kiefer, W. S., Taylor, G. J., Melosh, H. J., et al. (2013). The crust of the moon as seen by GRAIL. *Science*, *339*(6120), 671–675. https://doi.org/10.1126/science.1231530

Wilkins, S. J., & Gross, M. R. (2002). Normal fault growth in layered rocks at Split Mountain, Utah: Influence of mechanical stratigraphy on dip linkage, fault restriction and fault scaling. *Journal of Structural Geology*, *24*(9), 1413–1429. https://doi.org/10.1016/S0191-8141(01)00154-7

Wilson, L., & Head, J. W. (2018). Lunar floor-fractured craters: Modes of dike and sill emplacement and implications of gas production and intrusion cooling on surface morphology and structure. *Icarus*, *305*, 105–122. https://doi.org/10.1016/j.icarus.2017.12.030

Wojtal, S. F. (1996). Changes in fault displacement populations correlated to linkage between faults. *Journal of Structural Geology*, *18*(2–3), 265–279. https://doi.org/10.1016/S0191-8141(96)80049-6

Wyrick, D. Y., Morris, A. P., & Ferrill, D. A. (2011). Normal fault growth in analog models and on Mars. *Icarus*, *212*(2), 559–567. https://doi.org/10.1016/j.icarus.2011.01.011

Xu, S., Nieto-Samaniego, A. F., Murillo-Muñetón, G., Alaniz-Álvarez, S. A., Grajales-Nishimura, J. M., & Velasquillo-Martinez, L. G. (2016). Effects of physical processes and sampling resolution on fault displacement versus length scaling: The case of the Cantarell complex oilfield, Gulf of Mexico. *Pure and Applied Geophysics*, *173*(4), 1125–1142. https://doi.org/10.1007/s00024-015-1172-0